THE JOURNAL OF PHYSICAL CHEMISTRY C
A JOURNAL OF THE AMERICAN CHEMICAL SOCIETY

pubs.acs.org/JPCC

Article

Strongly Tunable Raman Resonance in InSe under Pressure

Ge Huang,[#] Yan Zhou,[#] Zuo-Yuan Dong, Wei-Jian Li, Ke-Jun Bu, Shi Zhou, Tao Wang, Xu-Jie Lü, and Xiao-Jia Chen*

Cite This: *J. Phys. Chem. C* 2022, 126, 6344−6350

Read Online

ACCESS | Metrics & More | Article Recommendations

ABSTRACT: The graphene-like layered semiconductor indium selenide has recently attracted widespread attention owing to its large tunability of the electronic states by varying layer thickness, chemical doping, or strain. However, the influence of the modulated inter- and intralayer chemical bonding upon lattice change on the optical and electrical properties is still in its infant stage. Here, we systematically investigate the high-pressure behaviors of the phonon modes and excitonic states in ε-InSe based on the measurements of Raman, absorption, and photoluminescence spectroscopy combined with theoretical calculations. We find drastically enhanced intensities ~3 orders of magnitude for the polar and high-order Raman modes. Such intensity enhancements of the Raman modes are found to arise from the near resonance between the laser photon energy and the exciton B in InSe with increasing pressure. Further analysis indicates unexpected weakening of the intralayer In−In bonds and a decrease of polarity of the In−Se bonds upon compression, thus leading to an increase in the energy of exciton B. These results also explain the nonlinear pressure-dependent band gap transition. We demonstrate that InSe provides a versatile platform from which to explore the practical applications in flexible electronic and optoelectronic devices.

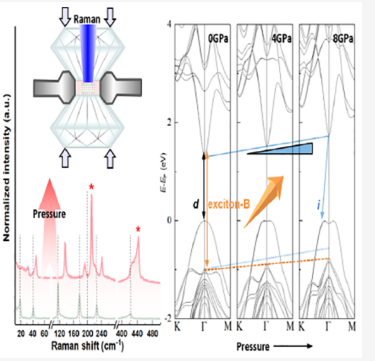

INTRODUCTION

Layered two-dimensional (2D) materials beyond graphene such as transition metal dichalcogenides, black phosphorus, and III−VI monochalcogenides have attracted tremendous interest for potential optoelectronic and electronic applications.[1−4] The anisotropic character of the interlayer and intralayer bonding gives rise to the large diversity of optical and electrical properties of the 2D materials.[5,6] For instance, monolayer and bulk rhenium disulfide (ReS_2) share similar electronic and vibrational properties because of the negligible interlayer interaction.[7] On the contrary, a sizable covalent interlayer interaction is illustrated in the black phosphorus, leading to the strongly layer-dependent band structures.[8,9] Therefore, tuning the degree of the anisotropy in the bonding upon lattice change can provide a great platform from which to modulate the physical properties of the 2D materials.[10,11] It is worth noting that monochalcogenides consist of a stack of 2D layers of two planes of metal atoms sandwiched between two chalcogen planes with a hexagonal symmetry. There exists distinct compressibility of the covalent cation−cation bond, the partially ionic cation−anion bond, and the van der Waals (vdW) coupled interlayer bonding. Such prolific bonding characteristics make monochalcogenides an ideal system to study the fundamental physics of the electronic states in 2D materials.

As a representative III−VI monochalcogenide, indium selenide (InSe) exhibits an extremely high carrier mobility, a dramatic photoresponse, and a large nonlinear effect.[4,12−15] Considerable studies have been put forward to investigate the uppermost valence bands of InSe for their participation in optical and transport properties. The topmost valence band with the dominance of the Se p_z orbital is pretty sensitive to the interlayer interaction for the orientation perpendicular to the layer surface.[16] With a decreasing number of layers, the band gap of InSe changes dramatically from 1.4 to 2.6 eV with the transition from a parabolic to ring-shaped topmost valence band.[17−20] Such a direct-to-indirect crossover can be interpreted on the basis of $k\cdot p$ theory due to the k-dependent orbital composition of the highest valence band.[21] A similar evolution of the band structures in InSe is also observed at high pressures.[22−26] Besides the band gap transition, there exists another interband transition (exciton B) near the Γ point between the lower-lying Se p_{xy} dominated valence bands and the In s dominated lowest conduction band.[27] It has been proven that exciton B can be involved in the resonant Raman transition to effectively detect the numbers of layers in InSe by using a single 514.5 nm laser.[28,29] In addition, exciton B enables InSe to efficiently absorb in-plane polarized light even with the nearly zero in-plane dipole matrix element for the

Received: February 7, 2022
Revised: March 19, 2022
Published: April 4, 2022

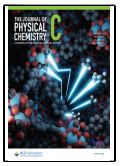

https://doi.org/10.1021/acs.jpcc.2c00913
J. Phys. Chem. C 2022, 126, 6344−6350

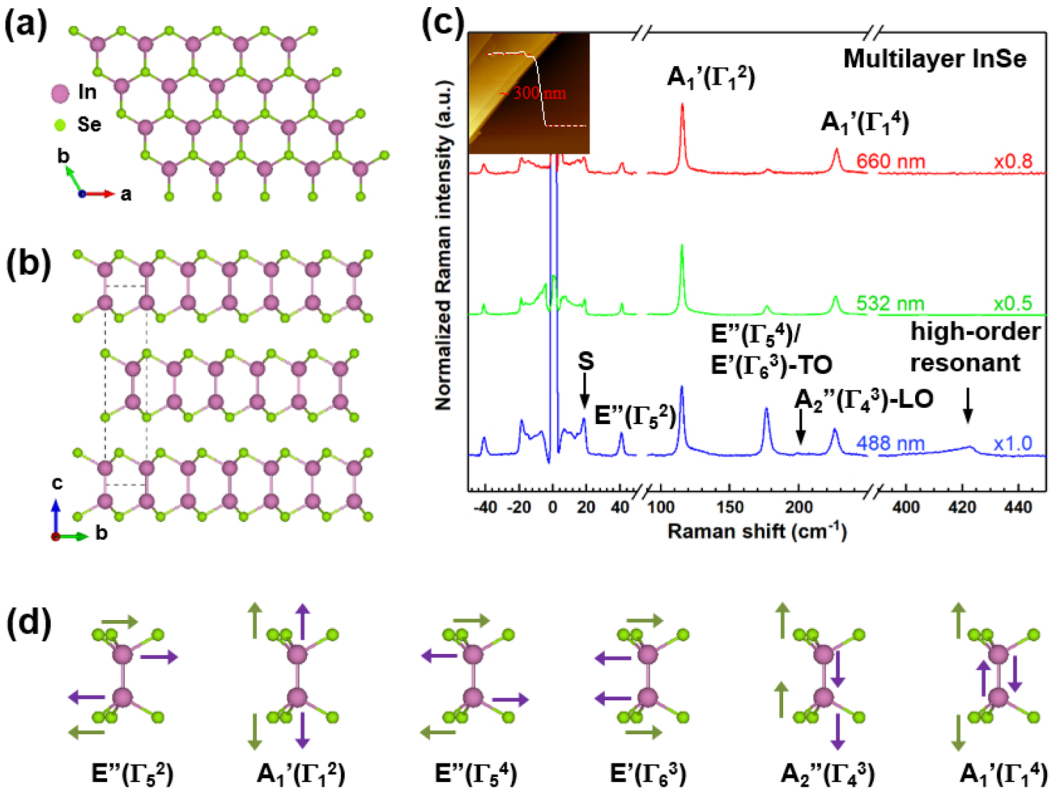

Figure 1. Top view (a) and side view (b) for ambient hexagonal structure ($P6_3/mmc$ symmetry) of InSe. (c) Representative Raman spectra of InSe under different wavelength excitations at room temperature. All observable Raman modes including the shear (S, 20 cm^{-1}) mode and the high-order resonant (404 and 425 cm^{-1}) modes are labeled. (Inset) The AFM image shows a height difference of 300 nm for the measured sample. (d) Schematic of symmetry of the phonon vibration modes experimentally observed in multilayer InSe. From left to right, the six vibrational schematics correspond to the first-order Raman modes observed at room temperature at 41, 115, 177, 177, 199, and 226 cm^{-1}, respectively.

fundamental band gap transition.[30,31] Both theoretical and experimental works have shown that transition B can be effectively tuned with a layer-dependent red-shift by the uniaxial tensile strain.[32,33] Therefore, it would be beneficial to explore the pressure effect on exciton B for possibly extending the spectral range in InSe. Moreover, it opens up an opportunity to better understand the inter- and intralayer contribution to the electronic states in InSe due to the significantly anisotropic compressibility.

In this work, we systematically investigate the vibrational and electronic properties of ε-InSe at pressures up to 9.8 GPa. ε-InSe belongs to the noncentrosymmetric space group D_{3h}^1 regardless of the number of layers.[34] Raman scattering measurements are conducted to monitor the high-pressure behaviors of the lattice vibrations and band structures. The absorption and photoluminescence spectroscopy, together with density functional theory (DFT) calculations, are performed to determine the pressure coefficients of the band gap and the exciton B. Overall, these efforts enable the determination of the role of the post-transition metal In atoms in tuning the energy width of exciton B at high pressures.

MATERIALS AND METHODS

The single-crystal bulk InSe ingot was grown by a horizontal gradient freeze method. Raw materials of high-purity powders of indium (In, 99.9999%, Alfa Aesar) and selenium (Se, 99.9999%, Alfa Aesar) were loaded into two similar pBN boats separately and placed in the two ends of an evacuated quartz ampule (more details of the growth method can be found in ref 35). Single-crystal InSe with dimensions of 10 × 10 × 3 mm^3 was cut from the InSe ingot. Ultrathin InSe multilayers were mechanically exfoliated from a single-crystal bulk InSe wafer onto diamond culets using Scotch tape. The thickness of the InSe multilayers was measured by atomic force microscopy (AFM, Oxford Instruments) and extracted from the tomography image using the tapping mode.

Pressure was generated via a symmetric diamond anvil cell (DAC) mounting a pair of type-Ia low-fluorescence diamonds with 300 μm diameter culets. A stainless steel gasket was preindented to a thickness of 30 μm and then laser-drilled centrally to produce a 150 μm diameter sample chamber. The neon was loaded into the sample chamber as the pressure-transmitting medium.

Pressures and their uncertainties were determined from the wavelength of the fluorescence peak of a ruby sphere placed close to the sample in the sample chamber of the DAC.[36] Raman measurements were performed using a Princeton Instruments spectroscopy system with a probe laser wavelength of 488, 532, or 660 nm. A 1800 L/mm grating was used to disperse the scattered light onto a charge-coupled device (CCD), resulting in a spectral resolution of 0.5 cm^{-1}. All Raman spectra in this work are collected by backscattering geometry. The Raman system was first calibrated using the characteristic 520.3 cm^{-1} peak of undoped single-crystal silicon with an uncertainty of 0.05 cm^{-1}. The incident laser power was stabilized <1 mW to avoid a heating effect, and the exposure time was 60 s. These laser parameters were kept the same during all of the measurements. Absorption spectra measure-

https://doi.org/10.1021/acs.jpcc.2c00913
J. Phys. Chem. C 2022, 126, 6344−6350

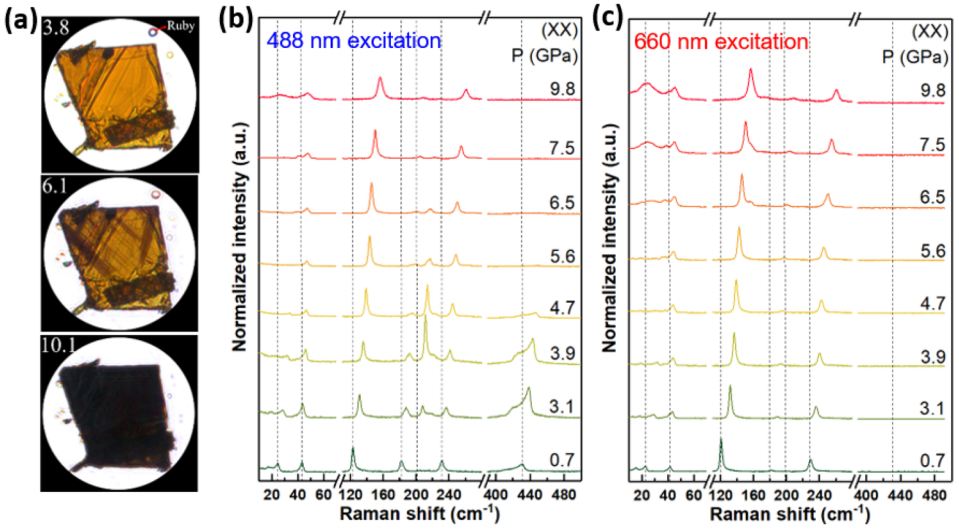

Figure 2. (a) Optical images of multilayer InSe under white light illumination taken at pressures of 3.8, 6.1, and 10.1 GPa. (b) Typical Raman spectra of InSe excited by a 488 nm laser and (c) a 660 nm laser as a function of pressure, with the excitation and the detection laser polarization parallel (XX) to the armchair direction of InSe. The vertical dashed lines are a guide for the eyes showing the evolution of the frequency of Raman modes with respect to the pressure.

ments were performed on single-crystalline InSe films via a home-built microspectroscopy system (Gora-UVN-FL, built by Ideaoptics, Shanghai, China). The exciton energy is determined from the $(\alpha h\nu)^2/(\alpha h\nu)^{0.5}$ versus $h\nu$ curve, where α is the absorption coefficient, h is the Planck constant, and ν is the frequency of the photon.

The density functional theory calculations were performed by using Vienna Ab Initio Simulation Package (VASP). The exchange-correlation energy function was determined using the Perdew–Burke–Ernzerhof form of the generalized gradient approximation (GGA-PBE).[37] For bulk parameter optimization, the van der Waals correction was applied by using optB88-vdW functionals.[38] The energy cutoff for the plane-wave basis was set to 520 eV, and the Brillouin zone was sampled using Γ-centered uniform Monkhorst–Pack (MP) meshes[39] with a resolution of $2\pi \times 0.02$ Å^{-1} in all calculations. The calculation continued until the total energy difference between consecutive cycles was $<10^{-7}$ eV and the maximum Hellmann–Feynman force was $<10^{-3}$ eV/Å.

RESULTS AND DISCUSSION

Bulk ε-InSe crystallizes in a hexagonal layered structure with space group $P\bar{6}m2$, as shown in Figure 1a and b. In comparison, γ-InSe has a 3R structure with an ABC stacking sequence, while β- and ε-InSe share a 2H structure with an AB stacking sequence and similar lattice parameters. Unlike the centrosymmetric feature that β-InSe has, ε-InSe possesses a noncentrosymmetric structure. The noncentrosymmetric structure feature with the In–In bonds perpendicular to the layers can also be distinguished in Figure 1b. The thickness of the InSe sample is determined to be ∼300 nm via atomic force microscopy measurements, as shown in the inset of Figure 1c.

To evaluate the ambient vibrational characteristics, we measured the Raman spectra of InSe under various wavelength laser excitations, as shown in Figure 1c. Notably, ε-InSe belongs to point group D_{3h}^1 and has four A_1' modes, four A_2'' modes, eight E' modes, and eight E'' modes.[40] As shown in Figure 1c, seven Raman peaks are observed, i.e., $E''(\Gamma_5^2)$ at 41 cm^{-1}, $A_1'(\Gamma_1^2)$ at 115 cm^{-1}, $E''(\Gamma_5^4)/E'(\Gamma_6^3)$-TO at 177 cm^{-1}, $A_1'(\Gamma_1^4)$ at 226 cm^{-1}, and high-order resonant modes of $2A_2''(\Gamma_4^3)$ and $A_2''(\Gamma_4^3) + A_1'(\Gamma_1^4)$ at 404 and 425 cm^{-1}, respectively. Moreover, the interlayer shear (S) mode can also be clearly observed at the low frequency of 20 cm^{-1}. With the near-resonant 488 nm excitation, we can also observe the weak $A_2''(\Gamma_4^3)$-LO mode at 199 cm^{-1}, which can be ascribed to the interaction between the polar phonon and the exciton B. The observation of the shear mode and the polar mode A_2''-LO can be assigned as the marker of the ε phase, as indicated by earlier works on InSe.[41,42] The schematic vibrations of the observed first-order modes are illustrated in Figure 1d.

Parts b and c of Figure 2 show the evolution of Raman spectra for InSe with respect to pressure excited under the 488 and 660 nm lasers, respectively. For the 488 nm laser excitation, we observed the greatly enhanced intensity of the $A_2''(\Gamma_4^3)$-LO and $E'(\Gamma_6^3)$-LO Raman modes, as well as the high-order resonant $2A_2''(\Gamma_4^3)$ and $A_2''(\Gamma_4^3) + A_1'(\Gamma_1^4)$ modes. Here, although all first-order Raman modes exhibit enhancements in the resonant condition, the enhancements of these resonant modes were 1–2 orders of magnitude stronger than the others. We focused on the drastically enhanced resonant modes. The intensities of the polar modes of $A_2''(\Gamma_4^3)$-LO and its accompanying broad shoulder increased gradually upon compression with a maximum appearing at a pressure of 3.9 GPa and then quenching quickly until disappearing at pressures over 7.5 GPa. Similar trends were also observed in the high-order Raman modes of $2A_2''(\Gamma_4^3)$ and $A_2''(\Gamma_4^3) + A_1'(\Gamma_1^4)$. However, their maximum intensities appeared at a relative low pressure of 2.5 GPa.

For the 660 nm laser excitation, no resonant modes appeared in the entire studied pressure region, except the slight enhancement in the relative intensity of the $A_1'(\Gamma_1^4)$ mode. It was also reported that, even at the excitation of the resonant photon energy (514.5 nm, 2.41 eV), no resonant Raman phenomenon was observed in γ-InSe at pressures <11 GPa.[43] This abnormal photon-energy-dependent resonance implied that the resonant conditions were unusually modified by pressure. Also, the subsequent saturation of the resonant modes at pressures <7 GPa indicated that the resonant states

https://doi.org/10.1021/acs.jpcc.2c00913
J. Phys. Chem. C 2022, 126, 6344–6350

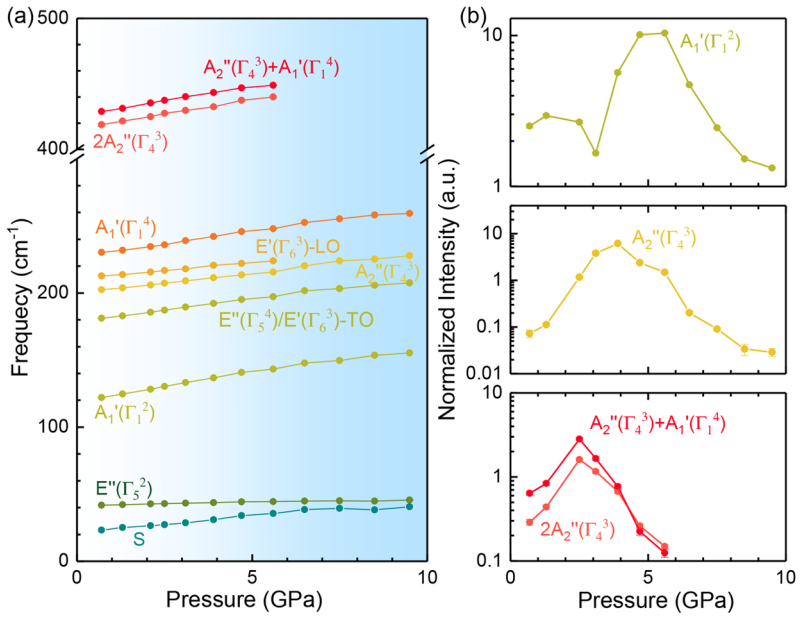

Figure 3. (a) Raman frequency shifts of all Raman modes as a function of pressure up to 13.5 GPa. The blue shaded rectangular indicates the entire intensity-enhancement region. (b) Evolution of the normalized intensity with pressure for the representative Raman modes with obvious enhancement.

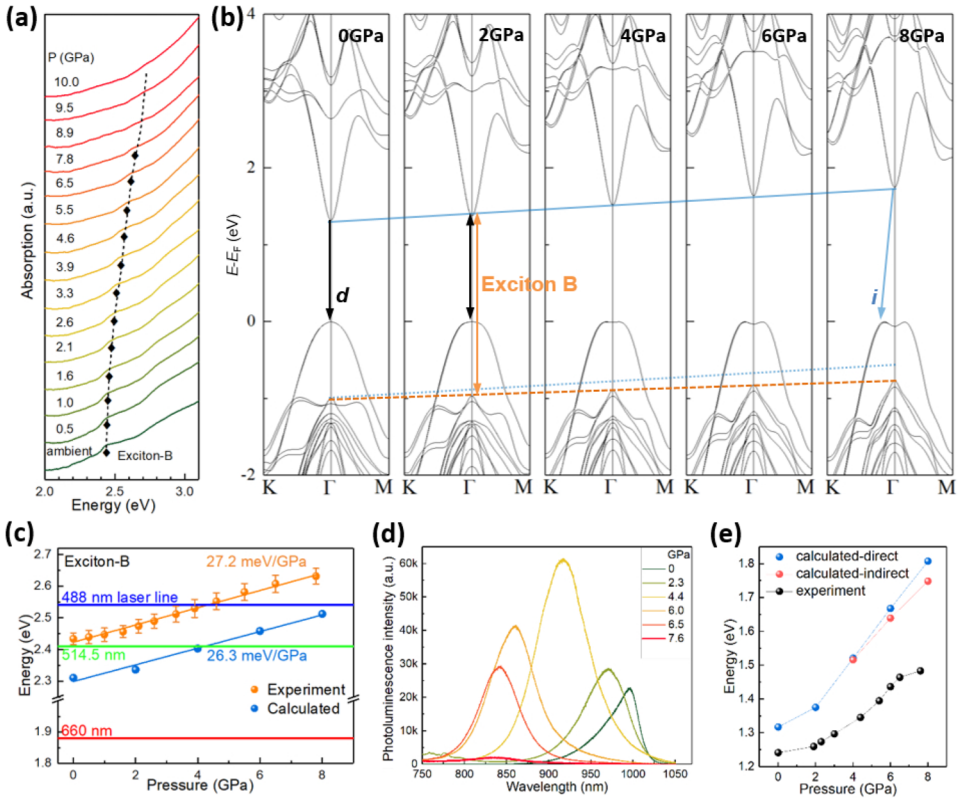

Figure 4. (a) Pressure-dependent visible-to-infrared absorption spectra, where the peak (labeled by the diamond symbol and dashed line) is ascribed to the exciton B absorption. Note that these curves taken at different pressures are vertically shifted for easier comparison. (b) Calculated band dispersion for the ε-InSe at high pressures. The direct-to-indirect bandgap transition is schematically labeled by *d* and *i*, respectively, together with the indication of the arrows. The blue and orange triangles represent the slope of energy with respect to pressure for CBM and sub-VBM, respectively. The transitions of the band gap and exciton B are also schematically labeled. (c) Pressure-dependent energy of exciton B extracted from both the experimental absorption spectra (orange points) and DFT theoretical (blue points) calculations. The blue, green, and red horizontal lines represent the photon energies of the 488, 514.5, and 660 nm lasesr, respectively. (d) Experimental evidence of the band-gap features at various pressures measured through high-pressure photoluminescence spectra. (e) Evolution of the experimental and calculated band gaps upon compression.

https://doi.org/10.1021/acs.jpcc.2c00913
J. Phys. Chem. C 2022, 126, 6344−6350

were gradually modulated by pressure. Previous studies showed that there was a structural change into the rock-salt phase at a pressure of 10 GPa.[44] The optical images in Figure 2a also show no obvious changes at 3.8 and 6.1 GPa, where the optimum and vanishing resonant modes appear, but the sample turned black at 10.1 GPa under the same measurement conditions, consistent with the pressure of the phase transition revealed in previous X-ray diffraction (XRD) experiments.[44] Therefore, the modulation of the resonant modes was not due to the structural transformation.

To gain a more in-depth understanding of the pressure dependence of the Raman modes of InSe, we analyzed the pressure-dependent frequency and intensity of all observable Raman modes (Figure 3). By using the Lorenz fitting to the measured Raman spectra, the frequency and intensity for each Raman mode were obtained. The evolution of the frequency with pressure is plotted in Figure 3a, where phonon strengthening was evident for almost all of the modes. Owing to the weak vdW interaction between the tetralayers, the crystal was much more compressible along the direction parallel to the c axis than thatparallel to the plane. Therefore, the out-of-plane vibrations such as $A_1'(\Gamma_1^2)$ and $A_1'(\Gamma_1^4)$ exhibited a highly pressure dependence in frequency.

With increasing pressure, the interlayer interaction would be strongly enhanced with decreasing distance between layers corresponding to the rapidly increasing frequency of the S mode. However, the low-frequency $E''(\Gamma_5^2)$ mode showed an insensitive characteristic to pressure. Displacements of this E'' mode are shown in Figure 1d. In the rigid layer approximation, the frequency of this E'' mode was determined by the interlayer force associated with a Se···Se bond as well as the intralayer bond-bending force. Consequently, the little variation of the frequency suggested that the large increase in the strength of the interlayer force was canceled by the weakening intralayer In−In bond-bending force.

For the polar E' mode, one may also note the slight approaching of the $E'(\mathrm{LO})$ mode and the $E'(\mathrm{TO})$ mode. It is worth noting that the splitting between the LO and TO phonons can be applied to obtain the Born effective charge.[45] Because the Born effective charge is a measure of the change of the electron distribution, the suppressed Born effective charge means decreasing bond polarity of the intralayer In−Se bond. Figure 3b shows the evolution of the normalized intensity for the typical Raman modes with increasing pressure. It is obvious that the intensities of all of the Raman modes were greatly enhanced at high pressures with a laser wavelength of 488 nm. However, we also note that the intensity of the polar Raman mode showed a more pronounced enhancement than other modes. Previous work has shown that the forbidden polar mode was due to the Fröhlich electron−phonon interaction.[46] Therefore, the scattering of the polar mode would show pretty strong outgoing resonance under resonant conditions. In addition, it also should be noted that the Raman modes exhibited different resonance behavior under pressure. As the phonon energy was increased from the $A_1'(\Gamma_1^2)$ to the second-order modes, the pressure of the Raman intensity peaks decreased. Therefore, it was suggested that the energy of exciton B increased with increasing pressure.

Thus, we conducted a series of infrared-to-violet absorption spectra of InSe to explore the pressure dependence of exciton B to understand the effect of resonant profiles on these phonon modes. Figure 4a shows a clear bump at ∼2.42 eV, corresponding to the energy of exciton B at ambient conditions. With increasing pressure, the energy of exciton B showed an anomalous blue-shift to higher energy states. Band dispersion via DFT calculations as shown in Figure 4b revealed similar increasing trends for the energy of both the band gap and exciton B at pressures ranging from 0 to 8 GPa. By comparing the evolution of these band structures with pressure, we found that the energy of the sub valence band maximum (sub-VBM) and the conduction band minimum (CBM) valley at the Γ-point increased quickly with increasing pressure. Also, the latter increased much faster upon compression. This made the energy of exciton B increase gradually and get closer to the energy of the incident photon (488 nm, 2.54 eV). Because DFT calculations normally underestimate the band gap, the scissor correction method was applied to the band-gap adjustment.[19,32] It can be expected that the calculated pressure-dependent energy of exciton B was still slightly lower than the experimentally measured values, as shown in Figure 4c. However, their energy shift rates as a function of pressure 27.2 meV/GPa from the experimental measurements and 26.3 meV/GPa from the theoretical predictions were quite close.

Figure 4c shows the gradually approaching resonant conditions at the fixed 488 nm excitation wavelength. When the energy of exciton B was increased closer to that of the 488 nm laser, the correlated intermediate electron/hole state gradually changed from a virtual to an active energy state. After the energy of exciton B was increased to larger than that of the 488 nm laser, the correlated Raman mode intensity gradually declined. Also, the crossover for the energy of the 488 nm laser and exciton B appeared at a pressure of ∼4 GPa. It was consistent with the position of the optimized resonance of the $A_2''(\Gamma_4^3)$ mode, where the largest enhancement of ∼3 orders of magnitude was achieved.

The pressure-dependent photoluminescence spectra of InSe were performed to further understand the pressure effect on the electronic states in InSe, as shown in Figure 4d. At ambient conditions, the emission spectra exhibited a broad spontaneous emission band at the energy of the direct band gap (1.24 eV). Upon further compression, the photoluminescence intensity decreased and vanished at a pressure >7.6 GPa, suggesting a direct-to-indirect band gap crossover. Figure 4e shows the pressure dependence of the direct and indirect edges in InSe from both the theoretical and experimental results. Despite the common underestimation of the band gap by DFT calculations, the nonlinear pressure dependence of the band gap transition was well-reproduced by the theoretical calculations, consistent with earlier studies.[47,48]

From the variation tendencies of the band structures in InSe, we can see that the larger rate of the upward shift for the conduction band minimum contributed to the addition of exciton B at high pressures. In addition, we also found a weakening intralayer In−In bond and a more covalent In−Se bond under pressure. Hence, the strongly strengthened In−Se bond interactions raised the antibonding In 5s conduction band, thus giving rise to the observed increase of exciton B. Such a scenario can also be applied to understand the nonlinear behaviors of band-gap transition upon compression. Because the interlayer distance decreased with increasing pressure, the vdW forces would be first strengthened, and thus the strong interlayer repulsion forces would dominate. It must be emphasized that the topmost Se p_z valence band showed an upward shift with enhanced interlayer interactions by increasing layers. On the other hand, the strengthening bond

https://doi.org/10.1021/acs.jpcc.2c00913
J. Phys. Chem. C 2022, 126, 6344−6350

interaction of the In−Se bonds lowered the energy of the bonding Se p_z valence band. Therefore, the modulation of both the intralayer bonding and the interlayer coupling effect was proposed to be responsible for the nonlinear increase in energy of the band-gap transition, agreeing well with the calculated band structures under pressure.

CONCLUSIONS

In summary, the evolution of the lattice vibrations and the electronic states, and their interactions in ε-InSe with increasing pressure, were systematically studied using Raman, absorption, and photoluminescence spectroscopy, as well as theoretical calculations. We observed drastic enhancements of ∼3 orders of magnitude of the Raman intensities for the forbidden longitudinal optical modes and high-order resonant modes. Such enhanced intensities of the Raman modes were found as a result of a near-resonance between the laser photon energy and the linear increase energy of exciton B with increasing pressure. By employing the DFT calculations, including the long-range dispersion interaction, the pressure-dependent band-gap values showed nonlinear behavior, agreeing well with the results obtained from the photoluminescence measurements. Therefore, with the application of pressure, the interlayer vdW forces as well as the intralayer In−In bond and In−Se bond could be significantly tuned, leading to versatile optical and electronic properties. The discovery also implies the great potential for applications in future flexible electronics and optoelectronics via pressure engineering in 2D materials.

AUTHOR INFORMATION

Corresponding Author

Xiao-Jia Chen − *Center for High Pressure Science and Technology Advanced Research, Shanghai 201203, P. R. China;* orcid.org/0000-0003-3921-9424; Email: xjchen@hpstar.ac.cn

Authors

Ge Huang − *Key Laboratory of Materials Physics, Institute of Solid State Physics, HFIPS, Chinese Academy of Sciences, Hefei 230031, P. R. China; University of Science and Technology of China, Hefei 230026, P. R. China; Center for High Pressure Science and Technology Advanced Research, Shanghai 201203, P. R. China;* orcid.org/0000-0002-1115-6620

Yan Zhou − *Center for High Pressure Science and Technology Advanced Research, Shanghai 201203, P. R. China*

Zuo-Yuan Dong − *Center for High Pressure Science and Technology Advanced Research, Shanghai 201203, P. R. China;* orcid.org/0000-0003-4441-649X

Wei-Jian Li − *Center for High Pressure Science and Technology Advanced Research, Shanghai 201203, P. R. China*

Ke-Jun Bu − *Center for High Pressure Science and Technology Advanced Research, Shanghai 201203, P. R. China*

Shi Zhou − *University of Science and Technology of China, Hefei 230026, P. R. China; State Key Laboratory of Solidification Processing, Northwestern Polytechnical University, Xi'an 710072, P. R. China*

Tao Wang − *State Key Laboratory of Solidification Processing, Northwestern Polytechnical University, Xi'an 710072, P. R. China; Research & Development Institute of Northwestern Polytechnical University, Shenzhen 518057, P. R. China;* orcid.org/0000-0003-3271-3331

Xu-Jie Lü − *Center for High Pressure Science and Technology Advanced Research, Shanghai 201203, P. R. China;* orcid.org/0000-0001-8402-7160

Complete contact information is available at: https://pubs.acs.org/10.1021/acs.jpcc.2c00913

Author Contributions

#G.H. and Y.Z. contributed equally.

Notes

The authors declare no competing financial interest.

ACKNOWLEDGMENTS

This work was funded through the National Key R& D Program of China (Grant no. 2018YFA0305900) at HPSTAR. T.W. acknowledges support by the Shenzhen Virtual University Park under Grant no. 2021Szvup110.

REFERENCES

(1) Xia, F. N.; Wang, H.; Xiao, D.; Dubey, M.; Ramasubramaniam, A. Two-dimensional material nanophotonics. *Nat. Photonics* **2014**, *8*, 899−907.

(2) Li, L.; Yu, Y.; Ye, G. J.; Ge, Q.; Ou, X.; Wu, H.; Feng, D.; Chen, X. H.; Zhang, Y. Black phosphorus field-effect transistors. *Nat. Nanotechnol.* **2014**, *9*, 372−377.

(3) Xia, F.; Wang, H.; Jia, Y. Rediscovering black phosphorus as an anisotropic layered material for optoelectronics and electronics. *Nat. Commun.* **2014**, *5*, 4458.

(4) Bandurin, D. A.; Tyurnina, A. V.; Yu, G. L.; Mishchenko, A.; Zólyomi, V.; Morozov, S. V.; Kumar, R. K.; Gorbachev, R. V.; Kudrynskyi, Z. R.; Pezzini, S.; et al. High electron mobility, quantum Hall effect and anomalous optical response in atomically thin InSe. *Nat. Nanotechnol.* **2017**, *12*, 223−227.

(5) Bradley, A. J.; Ugeda, M. M.; da Jornada, F. H.; Qiu, D. Y.; Ruan, W.; Zhang, Y.; Wickenburg, S.; Riss, A.; Lu, J.; Mo, S. K.; et al. Probing the role of interlayer coupling and coulomb interactions on electronic structure in few-layer $MoSe_2$ nanostructures. *Nano Lett.* **2015**, *15*, 2594−2599.

(6) Zhao, W.; Ghorannevis, Z.; Chu, L.; Toh, M.; Kloc, C.; Tan, P. H.; Eda, G. Evolution of Electronic Structure in Atomically Thin Sheets of WS_2 and WSe_2. *ACS Nano* **2013**, *7*, 791−797.

(7) Tongay, S.; Sahin, H.; Ko, C.; Luce, A.; Fan, W.; Liu, K.; Zhou, J.; Huang, Y. S.; Ho, C. H.; Yan, J.; et al. Monolayer behaviour in bulk ReS_2 due to electronic and vibrational decoupling. *Nat. Commun.* **2014**, *5*, 3252.

(8) Hu, Z. X.; Kong, X.; Qiao, J.; Normand, B.; Ji, W. Interlayer electronic hybridization leads to exceptional thickness-dependent vibrational properties in few-layer black phosphorus. *Nanoscale* **2016**, *8*, 2740−2750.

(9) Luo, X.; Lu, X.; Koon, G. K. W.; Castro Neto, A. H.; Özyilmaz, B.; Xiong, Q.; Quek, S. Y. Large frequency change with thickness in interlayer breathing mode-significant interlayer interactions in few layer black phosphorus. *Nano Lett.* **2015**, *15*, 3931−3938.

(10) Chi, Z. H.; Zhao, X. M.; Zhang, H.; Goncharov, A. F.; Lobanov, S. S.; Kagayama, T.; Sakata, M.; Chen, X. J. Pressure-induced metallization of molybdenum disulfide. *Phys. Rev. Lett.* **2014**, *113*, 036802.

(11) Ni, K.; Du, J.; Yang, J.; Xu, S.; Cong, X.; Shu, N.; Zhang, K.; Wang, A.; Wang, F.; Ge, L.; Zhao, J.; et al. Stronger interlayer interactions contribute to faster hot carrier cooling of bilayer graphene under pressure. *Phys. Rev. Lett.* **2021**, *126*, 027402.

(12) Lei, S.; Wen, F.; Ge, L.; Najmaei, S.; George, A.; Gong, Y.; Gao, W.; Jin, Z.; Li, B.; Lou, J.; et al. An atomically layered InSe avalanche photodetector. *Nano Lett.* **2015**, *15*, 3048−3055.

(13) Hao, Q. Y.; Yi, H.; Su, H. M.; Wei, B.; Wang, Z.; Lao, Z. Z.; Chai, Y.; Wang, Z. C.; Jin, C. H.; Dai, J. F.; et al. Phase identification and strong second harmonic generation in pure ε-InSe and its alloys. *Nano Lett.* **2019**, *19*, 2634−2640.
(14) Brotons-Gisbert, M.; Andres-Penares, D.; Suh, J.; Hidalgo, F.; Abargues, R.; Rodríguez-Cantó, P. J.; Segura, A.; Cros, A.; Tobias, G.; Canadell, E.; Ordejón, P.; et al. Nanotexturing to enhance photoluminescent response of atomically thin indium selenide with highly tunable band gap. *Nano Lett.* **2016**, *16*, 3221−3229.
(15) Dai, M.; Chen, H.; Wang, F.; Hu, Y.; Wei, S.; Zhang, J.; Wang, Z.; Zhai, T.; Hu, P. Robust Piezo-phototronic effect in multilayer γ-InSe for high-performance self-powered flexible photodetectors. *ACS Nano* **2019**, *13*, 7291−7299.
(16) Camara, M. O. D.; Mauger, A.; Devos, I. Electronic structure of the layer compounds GaSe and InSe in a tight-binding approach. *Phys. Rev. B* **2002**, *65*, 125206.
(17) Mudd, G. W.; Svatek, S. A.; Ren, T.; Patanè, A.; Makarovsky, O.; Eaves, L.; Beton, P. H.; Kovalyuk, Z. D.; Lashkarev, G. V.; Kudrynskyi, Z. R.; Dmitriev, A. I. Tuning the bandgap of exfoliated InSe nanosheets by quantum confinement. *Adv. Mater.* **2013**, *25*, 5714−5718.
(18) Mudd, G. W.; Molas, M. R.; Chen, X.; Zólyomi, V.; Nogajewski, K.; Kudrynskyi, Z. R.; Kovalyuk, Z. D.; Yusa, G.; Makarovsky, O.; Eaves, L.; et al. The direct-to-indirect band gap crossover in two-dimensional van der Waals indium selenide crystals. *Sci. Rep.* **2016**, *6*, 39619.
(19) Sun, Y.; Luo, S.; Zhao, X. G.; Biswas, K.; Li, S. L.; Zhang, L. InSe: a two-dimensional material with strong interlayer coupling. *Nanoscale* **2018**, *10*, 7991−7998.
(20) Hamer, M. J.; Zultak, J.; Tyurnina, A. V.; Zólyomi, V.; Terry, D.; Barinov, A.; Garner, A.; Donoghue, J.; Rooney, A. P.; Kandyba, V.; et al. Indirect to direct gap crossover in two-dimensional InSe revealed by angle-resolved photoemission spectroscopy. *ACS Nano* **2019**, *13*, 2136−2142.
(21) Rybkovskiy, D. V.; Osadchy, A. V.; Obraztsova, E. D. Transition from parabolic to ring-shaped valence band maximum in few-layer GaS, GaSe, and InSe. *Phys. Rev. B* **2014**, *90*, 235302.
(22) Segura, A.; Manjón, F. J.; Errandonea, D.; Pellicer-Porres, J.; Muñoz, V.; Tobias, G.; Ordejón, P.; Canadell, E.; San Miguel, A.; Sánchez-Portal, D. Specific features of the electronic structure of III-VI layered semiconductors: recent results on structural and optical measurements under pressure and electronic structure calculations. *Phys. Status Solidi B* **2003**, *235*, 267−276.
(23) Errandonea, D.; Segura, A.; Manjón, F. J.; Chevy, A.; Machado, E.; Tobias, G.; Ordejón, P.; Canadell, E. Crystal symmetry and pressure effects on the valence band structure of γ-InSe and ϵ-GaSe: Transport measurements and electronic structure calculations. *Phys. Rev. B* **2005**, *71*, 125206.
(24) Manjón, F. J.; Errandonea, D.; Segura, A.; Muñoz, V.; Tobías, G.; Ordejón, P.; Canadell, E. Experimental and theoretical study of band structure of InSe and $In_{1-x}Ga_xSe$ ($x < 0.2$) under high pressure: Direct to indirect crossovers. *Phys. Rev. B* **2001**, *63*, 125330.
(25) Segura, A. Layered Indium Selenide under High Pressure: A Review. *Crystals* **2018**, *8*, 206.
(26) Kuroda, N.; Ueno, O.; Nishina, Y. Supernonlinear Shifts of Optical Energy Gaps in InSe and GaSe under Hydrostatic Pressure. *J. Phys. Soc. Jpn.* **1986**, *55*, 581−589.
(27) Segura, A.; Bouvier, J.; Andrés, M. V.; Manjón, F. J.; Muñoz, V. Strong optical nonlinearities in gallium and indium selenides related to inter-valence-band transitions induced by light pulses. *Phys. Rev. B* **1997**, *56*, 4075−4084.
(28) Lei, S.; Ge, L.; Najmaei, S.; George, A.; Kappera, R.; Lou, J.; Chhowalla, M.; Yamaguchi, H.; Gupta, G.; Vajtai, R.; et al. Evolution of the electronic band structure and efficient photo-detection in atomic layers of InSe. *ACS Nano* **2014**, *8*, 1263−1272.
(29) Kuroda, N.; Nishina, Y. Resonant Raman scattering at higher M_0 exciton edge in layer compound InSe. *Solid State Commun.* **1978**, *28*, 439−443.
(30) Brotons-Gisbert, M.; Proux, R.; Picard, R.; Andres-Penares, D.; Branny, A.; Molina-Sánchez, A.; Sánchez-Royo, J. F.; Gerardot, B. D. Out-of-plane orientation of luminescent excitons in two-dimensional indium selenide. *Nat. Commun.* **2019**, *10*, 3913.
(31) Song, C.; Huang, S.; Wang, C.; Luo, J.; Yan, H. The optical properties of few-layer InSe. *J. Appl. Phys.* **2020**, *128*, 060901.
(32) Song, C.; Fan, F.; Xuan, N.; Huang, S.; Zhang, G.; Wang, C.; Sun, Z.; Wu, H.; Yan, H. Largely tunable band structures of few-layer InSe by uniaxial strain. *ACS Appl. Mater. Interfaces* **2018**, *10*, 3994−4000.
(33) Song, C.; Fan, F.; Xuan, N.; Huang, S.; Wang, C.; Zhang, G.; Wang, F.; Xing, Q.; Lei, Y.; Sun, Z.; et al. Drastic enhancement of the Raman intensity in few-layer InSe by uniaxial strain. *Phys. Rev. B* **2019**, *99*, 195414.
(34) Yang, Z.; Jie, W.; Mak, C. H.; Lin, S.; Lin, H.; Yang, X.; Yan, F.; Lau, S. P.; Hao, J. Wafer-Scale Synthesis of High-Quality Semiconducting Two-Dimensional Layered InSe with Broadband Photoresponse. *ACS Nano* **2017**, *11*, 4225−4236.
(35) Sun, M.; Wang, W.; Zhao, Q.; Gan, X.; Sun, Y.; Jie, W.; Wang, T. ϵ-InSe single crystals grown by a horizontal gradient freeze method. *CrystEngComm* **2020**, *22*, 7864−7869.
(36) Mao, H. K.; Bell, P. M.; Shaner, J. W.; Steinberg, D. J. Specific volume measurements of Cu, Mo, Pd, and Ag and calibration of the ruby R1 fluorescence pressure gauge from 0.06 to 1 Mbar. *J. Appl. Phys.* **1978**, *49*, 3276−3283.
(37) Perdew, J. P.; Burke, K.; Ernzerhof, M. Generalized gradient approximation made simple. *Phys. Rev. Lett.* **1996**, *77*, 3865−3868.
(38) Klimeš, J.; Bowler, D. R.; Michaelides, A. Chemical accuracy for the van der Waals density functional. *J. Phys.: Cond. Matt.* **2010**, *22*, 022201.
(39) Monkhorst, H. J.; Pack, J. D. Special points for Brillouin-zone integrations. *Phys. Rev. B* **1976**, *13*, 5188−5192.
(40) Allahverdi, K.; Babaev, S.; Ellialtioğlu, Ş; Ismailov, A. Raman scattering in layer indium selenide under pressure. *Solid State Commun.* **1993**, *87*, 675−678.
(41) Carlone, C.; Jandl, S.; Shanks, H. R. Optical Phonons and Crystalline Symmetry of InSe. *Phys. Status Solidi B* **1981**, *103*, 123−130.
(42) Chen, Z.; Biscaras, J.; Shukla, A. A high performance graphene/few-layer InSe photo-detector. *Nanoscale* **2015**, *7*, 5981−5986.
(43) Ulrich, C.; Mroginski, M. A.; Goñi, A. R.; Cantarero, A.; Schwarz, U.; Muñoz, V.; Syassen, K. Vibrational Properties of InSe under Pressure: Experiment and Theory. *Phys. Status Solidi B* **1996**, *198*, 121−127.
(44) Schwarz, U.; Goñi, A. R.; Syassen, K.; Cantarero, A.; Chevy, A. Structural and optical properties of InSe under pressure. *High Pressure Res.* **1992**, *8*, 396−398.
(45) Kuroda, N.; Ueno, O.; Nishina, Y. Lattice-dynamical and photoelastic properties of GaSe under high pressures studied by Raman scattering and electronic susceptibility. *Phys. Rev. B* **1987**, *35*, 3860−3870.
(46) Martin, R. M. Theory of the One-Phonon Resonance Raman Effect. *Phys. Rev. B* **1971**, *4*, 3676−3685.
(47) Goi, A. R.; Cantarero, A.; Schwarz, U.; Syassen, K.; Chevy, A. Low-temperature exciton absorption in InSe under pressure. *Phys. Rev. B* **1992**, *45*, 4221−4226.
(48) Manjón, F. J.; Segura, A.; Muñoz-Sanjosé, V.; Tobías, G.; Ordejón, P.; Canadell, E. Band structure of indium selenide investigated by intrinsic photoluminescence under high pressure. *Phys. Rev. B* **2004**, *70*, 125201.

https://doi.org/10.1021/acs.jpcc.2c00913
J. Phys. Chem. C 2022, 126, 6344−6350